IOSR Journal of Engineering (IOSRJEN) **www.iosrjen.org**
ISSN (e): 2250-3021, ISSN (p): 2278-8719
Vol. 08, Issue 6 (June. 2018), ||V (VI) || PP 01-14

MHD Double Diffusive Convective Heat Transfer Flow Of Micropolar Fluid In Cylindrical Annulus

Prof. C.Sulochana[1], Dr.K.Gnanaprasunamba[2]
[1]Department of Mathematics, Gulbarga University, Gulbarga, Karnataka, India
[2]Department of Mathematics, SSA Govt. First Grade College (Autonomous), Ballari, Karnataka, India
Corresponding Author: Dr.K.Gnanaprasunamba

Abstract: In this paper, combined influence of magnetic field and dissipation on connective heat and mass transfer flow of a viscous chemically reacting fluid through a porous medium in the concentric cylindrical annulus with inner cylinder maintained at constant temperature and concentration on the other cylinder maintained constant heat flux. The equations governing the flow, heat. Mass and micro rotation are solved by employing Galerkin finite element analysis with quadratic approximation functions. The temperature, concentration and micro concentration distributions are analyzed for different values of G, M, D^{-1}, R, S and Ec. The rate of heat and mass transfer and couple stress are numerically evaluated for different variations of the governing parameters.

Keywords: Heat and mass Transfer, Chemical reaction, Porous medium, Concentric Cylinder annulus, Micro polar Fluid.

Date of Submission: 07-06-2018 Date of acceptance: 26-06-2018

I. INTRODUCTION:

An enclosed cylindrical annular cavity formed by three vertical, concentric cylinders, containing a fluid through which heat is transferred by natural convection, is a simplified representation of a number of practical and experimental situations. Also, the annulus represents a common geometry employed in a variety of heat transfer systems ranging from simple heat exchangers to the most complicated nuclear reactors. Since, the flow and heat transfer in a cylindrical annular configuration contains all the essential physics that are common to all confined natural convective flows, a complete understanding of the flow in such geometry is very essential. In addition, from a computational stand point, the annular configuration allows investigation of a wide range of geometrical effects.

There have been widespread interests in the study of effect of magnetic field on natural convection in fluid saturated cylindrical porous annulus/annuli. Most of the studies found in literature on the effect of magnetic field on natural convection are mainly confined to rectangular enclosures or single cylindrical annulus in the presence and absence of porous medium. Sankar and Venkatachalappa [21] have investigated the effect of direction of magnetic field in a vertical cylindrical annulus. They showed that the radial magnetic field is more effective in suppressing the convection in tall cavities, while the axial magnetic field is more effective in suppressing the convection in tall cavities, while the axial magnetic field is effective in shallow cavities. Prasad and Kulacki [20] have studied the effect of free convection heat transfer in a liquid-filled vertical annulus. Shivakumara [22] have numerically investigated the natural convection in a vertical porous annulus using Darcy-Brinkmann model. Prasad *et al.* [18] have reported numerical results using Darcy equation for the case when a constant bottom portions are being insulated. Oreper and Szekely [17] reported the numerical computation of natural convection in a rectangular duct with electrically insulated walls in the presence of variable magnetic study to understand the effect of direction of magnetic field in cubical enclosure heated from one side wall and cooled from the opposite wall with all other walls are insulated. Later, Okada and Ozoe [16] studied the same problem experimentally using molten gallium (P_r = 0.024). They obtained the results under three different directions of magnetic field. They found that the external magnetic field, the vertical direction was found to be effective than the magnetic field applied parallel to the heated vertical wall. Also this observation is consistent with their numerical work.

Recently, Barletta *et al.* [2] studied mixed and forced convection Darcy flow in a vertical porous annulus around a straight electric cable by assuming fully developed parallel flow. The effect of magnetic field and internal heat generation on the free convection in a rectangular cavity filled with a porous medium is numerically investigated by Grosan *et al.* [8] for a wide range of physical parameters.

The theory of micropolar fluids initiated by Erigen [5] exhibits some microscopic effects arising from the local structure and micro motion of the fluid elements. Further, they can sustain couple stress and include classical Newtonian fluid as a special case. The model of micropolar fluid represents fluids consisting of rigid randomly oriented (or sphenical) particles suspended in a viscous medium where the deformation of the particles is ignored. The fluid containing certain additives, some polymeric fluids and animal blood are examples of micropolar fluids. The mathematical theory of equations of micropolar fluids and application of these fluids in the theory of lubrication and porous media is presented by Lukaszewics [12]. Agarwal and Dhanpal [1] obtained numerical solution of micropolar fluid flow and heat transfer between two co-axial porous circular cylinders.

Verma and Singh [27] have analyzed the behaviour of parametric fluid flow in a porous annulus in the presence of external magnetic field acting parallel to the common axis of the long co axial porous cylindrical tubes. Panja *et al.* [19] studied the flow of electrically conducting Reiner – Rivlin fluid between two non-conducting co axial circular cylinders with porous walls in the presence of uniform magnetic field. Shivashankar *et al.* [23] have obtained numerical solution to the MHD flow of micropolar fluid between two concentric porous cylinders; Murthy *et al.* [14] have considered study flow of micropolar fluid through a circular pipe and transverse with constant suction and injection.

All the above mentioned studies are based on the hypothesis that the effect of dissipation is neglected. This is possible in case of ordinary fluid flow like air and water under gravitational force. But this effect is expected to the relevant for fluids with high values of the dynamic viscosity flows. Moreover, Gebhart [10], Gebhart and Mollendorf [11] have shown that viscous dissipation heat in the natural convective flow is important when the flow field is of extreme size at extremely low temperature or in high gravitational field. On the other hand Barletta [3] have pointed out that relevant effects of viscous dissipation on the temperature profiles and on Nusselt number my occur in the fully developed forced convection in tubes. In view of this several authors notably Soundalgekar and Pop [26]. Soundalgekar *et al.* [24], Barletta and Zandhicn [4], Sreevani [25], El-Hakein [6] and Barletta [3] have studied the effect of viscous dissipation on the convective flows past an infinite vertical plate and through vertical channels and ducts. The effect of viscous dissipation on natural convection has been studied for some different cases including the natural convection from horizontal cylinder embedded in a porous media by Fand and Brucker [7], Giampietrao Fabbn [9] and Sreevani [25]. They reported that the viscous dissipation may not be neglected in all cases of natural convection from horizontal cylinders and further that the inclusion of a viscous dissipation term in a porous medium may lead to more accurate correlation equations, the effect of viscous dissipation has been studied by Nakayama and Pop [15] for steady free convection boundary layer over a non-isothermal body of arbitrary shape embedded in porous media. They used the integral method to show that the viscous dissipation results in lowering the level of the heat transfer rate from the body. This observation has been pointed also by Murthy and Singh [13] for the natural connection flow along an isothermal wall embedded in a porous medium. They concluded that that the effect of viscous dissipation increases as we move from Non-Darcy regime to Darcy regime.

II. FORMULATION OF THE PROBLEM:

We consider the steady flow of an incompressible, viscous, electrically conducting micropolar fluid through a porous medium in an annulus region between the concentric porous cylinders r = a and r = b (b > a) under the influence of a radial magnetic field $\frac{H_0}{r^2}$.

The fluid is injected through the inner cylinder with radial velocity u_b and flows outward through the outer cylinder with a radial velocity u_a. We also take the viscous, Darcy and Ohmic dissipation into account

The velocity and micro rotation are taken in the form

$$\left.\begin{aligned} &v_r = u(r), v_\theta = v = 0, \quad v_z = w(r) \\ &\omega_r = 0, \quad \omega_\theta = \omega(r), \quad \omega_z = 0 \end{aligned}\right\} \tag{3.1}$$

The equations governing the flow and heat and mass transfer (3.1)

$$\frac{\partial u}{\partial r} + \frac{u}{r} = 0$$

$$\rho u \frac{\partial u}{\partial r} = -\frac{\partial \phi}{\partial r} + (\mu + k)\left(\frac{\partial^2 u}{\partial r^2} + \frac{1}{r}\frac{\partial u}{\partial r} - \frac{u}{r^2}\right) - \left(\frac{\mu}{k_1}\right)u \tag{3.2}$$

$$\rho u\frac{\partial w}{\partial r}=-\frac{\partial p}{\partial z}+(\mu+k)\left(\frac{\partial^2 w}{\partial r^2}+\frac{1}{r}\frac{\partial w}{\partial r}\right)-\rho\bar{g}-\left(\frac{\mu}{k_1}\right)w$$

$$-k\frac{\partial w}{\partial r}(r\omega)-\frac{\sigma\mu_e^2H_0^2}{r^2}w \qquad (3.3)$$

$$\rho ju\frac{\partial\omega}{\partial r}=r\left(\frac{\partial^2\omega}{\partial r^2}+\frac{1}{r}\frac{\partial\omega}{\partial r}-\frac{N}{r^2}\right)-k\frac{\partial w}{\partial r}-2k\omega \qquad (3.4)$$

$$\rho_0C_pw\frac{\partial T}{\partial z}=k_f\left(\frac{\partial^2 T}{\partial r^2}+\frac{1}{r}\frac{\partial T}{\partial r}\right)+(2\mu+k)\left[\left(\frac{\partial u}{\partial r}\right)^2+\frac{\mu^2}{r^2}+\frac{1}{2}\left(\frac{\partial w}{\partial r}\right)^2\right]$$

$$+2k\left(\frac{1}{2}\frac{\partial w}{\partial r}+\omega\right)^2-2\frac{\beta}{r}\omega\frac{\partial\omega}{\partial r}+r\left(\left(\frac{\partial\omega}{\partial r}\right)^2+\frac{\omega^2}{r^2}\right) \qquad (3.5)$$

$$w\frac{\partial C}{\partial z}=D_m\left(\frac{\partial^2 C}{\partial r^2}+\frac{1}{r}\frac{\partial C}{\partial r}\right)-\gamma' C \qquad (3.6)$$

$$\rho-\rho_o=-\beta\rho_o(T-T_o)-\beta^\bullet\rho_o(C-C_o) \qquad (3.7)$$

where u, w are the velocity components along 0(r, z) directions, T is the temperature, ω is the micro rotation, p is the pressure, ρ is the density, μ is the dynamic viscosity, C_p is the specific heat at constant pressure, k_f is the thermal conductivity, k_1 is the permeability of the porous permeability, σ is the electrical conductivity μ is the magnetic permeability and k, r, β are the material constants.

The boundary conditions are

$u = ub$, $w = 0$, $\omega = 0$, $T = T_0 + A_0 z$, $C = C_0 + B_0 z$ on $r = a$

$u = ua$, $w = 0$, $\omega = 0$, $T = T_1 + A_0 z$, $C = C_1 + B_0 z$ on $r = b$

From the equation of continuity we obtain

$ru = c$, constant $\Rightarrow ru = au_a = bu_b$

$$\Rightarrow u=\frac{au_a}{r}$$

In view of the boundary condition on temperature and concentration, we may write

$T = T_0 + A_0(z) + \theta(r)$, $C = C_0 + B_0(z) + \phi(r)$

On introducing the non-dimensional variables r′, w′, θ′, p′ and N′ as

$$r'=\frac{r}{a},w'=\frac{w}{\nu/a},\theta=\frac{T-T_0}{T_i-T_0},\omega'=\frac{(\mu+k)\omega}{\rho\left(\mu^2/a^2\right)},p'=\frac{p}{\rho\left(\mu^2/a^2\right)},\phi=\frac{C-C_0}{C_i-C_0}$$

The equations (3.2) – (3.4) reduces to (on dropping the dashes)

$$w_{rr}+\left(1-\frac{S}{1+\Delta}\right)\frac{1}{r}w_r=-\pi_1+\frac{M^2}{r^2}w+D_1^{-1}w-G_1(\theta+N\phi)-\frac{\Delta_1}{r}\frac{\partial}{\partial r}(r\omega)$$

$$\omega_{rr}+(1-SA)\frac{1}{r}\omega_r-\left(\frac{1}{r^2}-\frac{2\Delta}{A}\right)\omega=\frac{\Delta_1}{Ar}\frac{dw}{dr} \qquad (3.8)$$

$$P_rN_Tw=\theta_{rr}+\frac{1}{r}\theta_r+EcP_r\left\{\begin{array}{c}(2+\Delta)\left(\frac{S^2}{r^4}+w_r^2\right)+2\Delta\left(\frac{1}{2}w_r+\omega\right)^2\\-2\Delta\omega\frac{\partial\omega}{\partial r}+A_1\left(w_r^2+\frac{\omega^2}{r^4}\right)\end{array}\right\} \qquad (3.9)$$

$$Sc\, N_c w = \phi_{rr} + \frac{1}{r}\phi_r - \gamma\,\phi$$

Where

$G = \dfrac{\beta g a^3 \Delta T}{\nu^2}$ (Grashof number),

$D^{-1} = \dfrac{a^2}{k_1}$ (Darcy parameter)

$P_r = \dfrac{\mu C_p}{k_f}$ (Prandtl number),

$Ec = \dfrac{a^2}{C_p \Delta T \nu^2}$ (Eckert number)

$M^2 = \dfrac{\sigma \mu_e^2 H_0^2 a^2}{\nu^2}$ (Hartmann number),

$S = \dfrac{a u_a}{\nu}$ (Suction parameter)

$\gamma = \dfrac{\gamma' a^2}{D_m}$ (Chemical Reaction parameter),

$A = \dfrac{r}{\mu a^2}$ $\quad \Delta = \dfrac{\mu}{k}$ (Micropolar parameters)

$$\Delta_1 = \frac{\Delta}{1+\Delta}, \quad D_1^{-1} = \frac{D^{-1}}{1+\Delta}, \quad G_1 = \frac{G}{1+\Delta}, \quad M_1^2 = \frac{M^2}{1+\Delta}, \quad r = \frac{b}{a}$$

The non-dimensional boundary conditions are

$$w = 0, \quad \theta = 1, \quad \phi = 1 \quad N = 0 \quad \text{on} \quad r = 1$$

$$w = 0, \quad \theta = 0, \quad \phi = 0 \quad N = 0 \quad \text{on} \quad r = s \tag{3.10}$$

III. METHOD OF SOLUTION:

Finite Element Analysis:

The finite element analysis with quadratic polynomial approximation functions is carried out along the radial distance across the circular cylindrical annulus. The behavior of the velocity, temperature and concentration profiles has been discussed computationally for different variations in governing parameters. The Gelarkin method has been adopted in the variation formulation in each element to obtain the global coupled matrices for the velocity, temperature and concentration in course of the finite element analysis. Choose an arbitrary element e_k and let w^k, θ^k and N^k be the values of w, θ and N in the element e_k.

We define the error residuals as

$$E_w^k = \frac{d}{dr}\left(r\frac{dw^k}{dr}\right) - \frac{\lambda}{1+\Delta}\frac{dw^k}{dr} + \Delta_1(r\omega^k) + \pi_1 r - \frac{M^2}{r}w^k + D^{-1}rw^k - Gr(\theta^k + N\phi^k) \tag{3.11}$$

$$E_\theta^k = \frac{d}{dr}\left(r\frac{d\theta^k}{dr}\right) - P_r N_t w_r + EcP_r\left\{\begin{array}{l}(2+\Delta)\dfrac{\lambda^2}{r^3} + ((2+\Delta)r + A)\left(\dfrac{dw}{dr}\right)^2 + \\ 2\Delta r\left(\dfrac{1}{2}\dfrac{dw}{dr} + \right)^2 \omega - 2A\omega\dfrac{d\omega}{dr} + A_1\dfrac{\omega^2}{r}\end{array}\right\} \tag{3.12}$$

$$E_C^k = \frac{d}{dr}\left(r\frac{d\phi^k}{dr}\right) - ScN_C w_r - \gamma\phi^l + EcP_r \left\{ \begin{array}{l} (2+\Delta)\frac{\lambda^2}{r^3} + ((2+\Delta)r + A)\left(\frac{dw}{dr}\right)^2 + \\ 2\Delta r\left(\frac{1}{2}\frac{dw}{dr} + \omega\right)^2 - 2A\omega\frac{d\omega}{dr} + A_1\frac{\omega^2}{r} \end{array} \right\}$$

$$E_N^k = \frac{d}{dr}\left(r\frac{d\omega^k}{dr}\right) - \omega A r\frac{d\omega^k}{dr} - \left(\frac{1}{r} - \frac{2\Delta r}{A}\right)\omega^k - \frac{\Delta}{A}\frac{dw^k}{dr} \qquad (3.13)$$

Where w^k, θ^k and ω^k are values of w, θ and ω in the arbitrary element e_k. These are expressed as linear combinations in terms of respective local nodal values.

$$w^k = w_1^k\psi_1^k + w_2^k\psi_2^k + w_3^k\psi_3^k = \sum_{i=1}^{3} w_i^k\psi_i^k$$

$$\theta^k = \theta_1^k\psi_1^k + \theta_2^k\psi_2^k + \theta_3^k\psi_3^k = \sum_{i=1}^{3} \theta_i^k\psi_i^k$$

$$\omega^k = \omega_1^k\psi_1^k + \omega_2^k\psi_2^k + \omega_3^k\psi_3^k = \sum_{i=1}^{3} \omega_i^k\psi_i^k$$

Where $\psi_1^k, \psi_2^k, \ldots$ etc are Lagrange's quadratic polynomials.

Following the Gelarkin weighted residual method and integrating by parts (3.11) – (3.13) we obtain

$$\int_{r_A}^{r_B} r\frac{dw^k}{dr}\frac{d\psi_j^k}{dr}dr - \frac{S}{1+\Delta}\int_{r_A}^{r_B}\frac{dw^k}{dr}\psi_j^k dr + \Delta_1 r\int_{r_A}^{r_B}\omega^k\psi_j^k + \pi_1\int_{r_A}^{r_B} r\,\psi_j^k dr -$$
$$\int_{r_A}^{r_B}\frac{M^2}{r}w^k\psi_j^k dr + \int_{r_A}^{r_B} D^{-1} r w^k\psi_j^k - G\int_{r_A}^{r_B} r(\theta^k + N\phi^k)\psi_j^k dr = Q_{2.j}^k + Q_{1.j}^k \qquad (3.14)$$

Where

$$-\theta_{1,J}^k = \left[\left(\frac{dw^k}{dr}\right)\left(r\psi_J^k\right)\right]_{rA} + \left[(\omega^k + \theta^k)\psi_j^k\right]_{rA}$$

$$-\theta_{2,J}^k = \left[\left(\frac{dw^k}{dr}\right)\left(r\psi_J^k\right)\right]_{r_B} + \left[(\omega^k + \theta^k)\psi_J^k\right]_{rB}$$

$$\int_{r_A}^{r_B} r\frac{d\theta^k}{dr}\frac{d\psi^2}{dr}dr = P_r N_t\int_{r_A}^{r_B} r w^k\psi_j^k dr + R_{2J}^k + R_{1J}^k +$$
$$EcP_r\left\{\begin{array}{l} (2+\Delta)\int_{r_A}^{r_B}\frac{\lambda^k}{r^3}\psi_j^k dr + [(2+\Delta)r + A]\int_{r_A}^{r_B}\left(\frac{dw^k}{dr}\right)^2\psi_j^k dr + 2\Delta r \\ \int_{r_A}^{r_B}\left(\frac{1}{2}\frac{dw^k}{dr} + \omega^k\right)^2\psi_j^k dr - 2A\int_{r_A}^{r_B}\omega^k\frac{d\omega^k}{dr}\psi_j^k dr + A_1\int_{r_A}^{r_B}\frac{(\omega^k)^2}{r}\psi_j^k dr \end{array}\right\} \qquad (3.15)$$

Where

$$-R_{1J}^k = \left(\frac{d\theta^k}{dr}(r\psi_J^k)\right)_{rA} + \left[w^k(r\psi_J^k)\right]_{rA} + \left[\omega^k(r\psi_J^k)\right]_{rA}$$

$$-R_{2J}^k = \left(\frac{d\theta^k}{dr}(r\psi_J^k)\right)_{rB} + \left[w^k(r\psi_J^k)\right]_{rB} + \left[\omega^k(r\psi_J^k)\right]_{rB}$$

$$\int_{r_A}^{r_B} r\frac{d\omega^k}{dr}\frac{d\psi_j^k}{dr}dr = SAr\int_{r_A}^{r_B}\frac{d\omega^k}{dr}\psi_j^k dr + \int_{r_A}^{r_B}\left(\frac{1}{r}-\frac{2\Delta r}{A}\right)\omega^k\psi_j^k dr \qquad (3.16)$$

$$S_{2j}^k + S_{1j}^k + \frac{\Delta}{A}\int_{r_A}^{r_B}\frac{d\omega^k}{dr}\psi_j^k dr$$

Where $-S_{1J}^k = \left(\left(\frac{d\omega^k}{dr}\right)(r\psi_J^k)\right)_{rA}$,

$$S_{2J}^k = \left(\left(\frac{d\omega^k}{dr}\right)(r\psi_J^k)\right)_{rB}$$

Expressing w^k, θ^k, N^k in terms of local nodal values in (3.14) – (3.16) we obtain

$$\left.\begin{aligned}&\sum_{i=1}^{3} w^k\int_{r_A}^{r_B}\frac{d\psi_i^k}{dr}\frac{d\psi_j^k}{dr}dr - \frac{\lambda}{1+\Delta}\sum_{i=1}^{3} w^k\int_{r_A}^{r_B}\frac{d\psi_i^k}{dr}\psi_j^k dr\\ &+\Delta_1\sum_{i=1}^{3}\omega^k\int_{r_A}^{r_B} r\psi_i^k\psi_j^k dr + \sum_{i=1}^{3}\pi_i\int_{r_A}^{r_B} r\psi_i^k\psi_j^k dr\\ &-M^2\sum_{i=1}^{3} w^k\int_{r_A}^{r_B}\frac{1}{r}\psi_i^k\psi_j^k dr + D_1^{-1}\sum_{i=1}^{3} w^k\int_{r_A}^{r_B} r\psi_i^k\psi_j^k dr\\ &-G_1\sum_{i=1}^{3}(\theta^k + N\phi^k)\int_{r_A}^{r_B} r\psi_i^k\psi_j^k dr = Q_{2J}^k + Q_{1J}^k\end{aligned}\right\} \qquad (3.17)$$

$$\begin{aligned}&\sum_{i=1}^{3}\theta^k\int_{r_A}^{r_B} r\frac{d\psi_i^k}{dr}\frac{d\psi_j^k}{dr}dr - N_t P_r\sum_{i=1}^{3} w^k\int_{r_A}^{r_B} r\psi_i^k\psi_j^k dr\\ &-EcP_r\left\{\begin{aligned}&(2+\Delta)\sum_{r=1}^{3}\int_{r_A}^{r_B}\frac{\lambda^2}{r^3}\psi_i^k\psi_j^k dr\\ &+\left[(2+\Delta)r + A\right]\sum_{i=1}^{3} w^{k^2}\int_{r_A}^{r_B}\left(\frac{d\psi_i^k}{dr}\right)\psi_j^k dr\\ &+2\Delta r\sum_{i=1}^{3}(w^k+\omega^k)^2\int_{r_A}^{r_B}\left(\frac{1}{2}\frac{d\psi_i^k}{dr}+\omega_i^k\right)^2\psi_j^k dr\\ &-2AN\sum_{i=1}^{3}\omega^k\int_{r_A}^{r_B}\frac{d\psi_i^k}{dr}\psi_j^k dr + A_1\sum_{r=1}^{3}\int_{r_A}^{r_B}\frac{\omega^2}{r}\psi_i^k\psi_j^k dr\end{aligned}\right\} = R_{2J}^k + R_{1J}^k\end{aligned} \qquad (3.18)$$

$$\begin{aligned}&\sum_{i=1}^{3}\omega^k\int_{r_A}^{r_B} r\frac{d\psi_i^k}{dr}\frac{d\psi_j^k}{dr}dr - SA\sum_{i=1}^{3}\omega^k\int_{r_A}^{r_B} r\frac{d\psi_i^k}{dr}\psi_j^k dr\\ &-\sum_{i=1}^{3}\omega^k\int_{r_A}^{r_B}\left(\frac{1}{r}-\frac{2\Delta r}{A}\right)\psi_i^k\psi_j^k dr - \frac{\Delta}{A}\sum_{r=1}^{3} w^k\int_{r_A}^{r_B}\frac{d\psi_i^k}{dr}\psi_i^k dr = S_{2J}^k + S_{1J}^k\end{aligned} \qquad (3.19)$$

Choosing different Ψ_j^k's corresponding to each element e_k in the equation (3.17) yields a local stiffness matrix of order 3×3 in the form

$$\left(f_{iJ}^{k}\right)\left(w_{i}^{k}\right)-\delta G_{1}\left(g_{ij}^{k}\right)\left(\theta_{i}^{k}+N\omega_{i}^{k}\right)+\delta D_{1}^{-1}\left(m_{iJ}^{k}\right)\left(u_{i}^{k}\right)+\delta^{2}A\left(n_{iJ}^{k}\right)\left(u_{i}^{k}\right)=\left(Q_{2J}^{k}\right)+\left(Q_{1J}^{k}\right)+\left(v_{j}^{k}\right) \quad (3.20)$$

Likewise the equation (3.18) and (3.19) gives rise to stiffness matrices

$$\left(e_{iJ}^{k}\right)\left(\theta_{i}^{k}\right)-N_{t}\,P_{r}\left(t_{iJ}^{k}\right)\left(w_{i}^{k}\right)=R_{2J}^{k}+R_{1J}^{k} \quad (3.21)$$

$$\left(l_{iJ}^{k}\right)\left(\omega_{i}^{k}\right)-N_{2}C\left(t_{iJ}^{k}\right)\left(w_{i}^{k}\right) \quad (3.22)$$

Where

$\left(f_{iJ}^{k}\right),\left(g_{iJ}^{k}\right),\left(m_{iJ}^{k}\right),\left(n_{iJ}^{k}\right),\left(e_{iJ}^{k}\right),\left(l_{iJ}^{k}\right)$ and $\left(t_{iJ}^{k}\right)$ are 3×3 matrices and $V_{j}^{k}=-P_{1}\int_{rA}^{rB} r\psi_{i}^{k}\psi_{j}^{k}dr$ and $\left(Q_{2J}^{k}\right),\left(Q_{1J}^{k}\right),\left(R_{2J}^{k}\right),\left(R_{1J}^{k}\right),\left(S_{2J}^{k}\right)$ and $\left(S_{1J}^{k}\right)$ are 3×1 column matrices and such stiffness (3.20) – (3.22) in terms of local nodes in each element are assembled using inter element continuity and equilibrium conditions to obtain the coupled global matrices in terms of the global nodal values of w, θ, ϕ and ω. In case we choose n-quadratic elements then the global matrices are of order 2n+1. The ultimate coupled global matrices are solved to determine the unknown global nodal values of the velocity, temperature and concentration in fluid region. In solving these global matrices an iteration procedure has been adopted to include the boundary and effects in the porous region.

In fact, the non-linear term arises in the modified Brinkman Linear momentum equation (3.14) of the porous medium. The iteration procedure in taking the global matrices as follows, we split the square term into a product term and keeping one of them say u_i's under integration. The other is expanded in terms of local nodal values as in (3.16), resulting in the corresponding coefficient matrix $(n_{iJ}^{k}\text{'}S)$ in (3.18), whose coefficients involve the in known u_i's To evaluate (3.19) to begin with choose the initial global nodal values of w_i's as zeros in the zeroth approximation, we evaluate w_i's, θ_i's, ϕ_i's and ω_i's in the usual procedure mentioned earlier. Later choosing these values of w_i's as first order approximation calculate θ_i's ϕ_i's and ω_i's. In the second iteration, we substitute for w_i's the first order approximation. This procedure is repeated till the consecutive values of w_i's, θ_i's, ϕ_i's and ω_i's differ by a pre-assigned percentage. For computational purpose we choose five elements in flow region.

IV. STIFFNESS MATRICES:

The global matrix for θ is

$A_1 X_1 = B_1$ (3.23)

The global matrix for N is

$A_2 X_2 = B_2$ (3.24)

The global matrix w is

$A_3 X_3 = B_3$ (3.25)

The global matrix *a* is

$A_4 X_4 = B_4$ (3.26)

The shear stress (τ) is evaluated using the formula $\tau=\left(\frac{du}{dr}\right)_{r=1,S}$

The rate of heat transfer (Nusselt number) is evaluated using the formula

$$Nu=-\left(\frac{d\theta}{dr}\right)_{r,S}$$

The couple stress at the inner and outer cylinder are evaluated by

$$M^{*}=-\left(\frac{dN}{dr}\right)_{r,S}$$

For M=0 the results are in good agreement with Agarwal and Dhanpal [1].

V. RESULTS AND DISCUSSION:

In this analysis we investigate the effect of dissipation and chemical reaction on mixed convective heat and mass transfer flow of a micro polar fluid through a porous medium in circular annulus between the cylinders r=a and r=b which are maintained at constant temperature and concentration. The non-linear coupled equations governing the flow heat and mass transfer are solved by Galerkine finite element analysis with quadratic appro functions. The Prandtl number Pr, material constants A and A_1 are taken to be constant at 0.733, 1 and 1 respectively where as the effect of other important parameters namely micro polar parameter Δ, the suction Reynolds number λ, Grashof number G, buoyancy ratio N, Inverse Darcy parameter D^{-1} and Schmidt number Sc has been studied for these functions and corresponding profiles are shown in Figs.

Fig. 1 represents w with Darcy parameter D^{-1}. It is found that lesser the permeability of porous medium larger |w| in the flow region. Fig represents w with chemical reaction parameter γ. It is found that the magnitude of w enhances in both the degenerating and generating chemical reaction cases. The non-dimensional temperature (θ) is exhibited in Figs for different parametric values. It is found that the non-dimensional temperature is always positive for all variations. This indicates the actual temperature is always greater than T_0. Fig. 2 represents θ with D^{-1}. It can be seen from the profiles that the actual temperature reduces with increase in D^{-1}. Fig.6 represents θ with chemical reaction parameter γ. It is found that the actual temperature enhances with γ in both degenerating and generating cases. The variation of θ with Eckert number Ec is shown in the Fig. 9. It is found that the actual temperature reduces with Ec in the region 1.2-1.5 and enhances in the region 1.6-1.9. The concentration distribution (C) is exhibited in Figs. We follow the convention that the non-dimensional concentration distribution is positive or negative according as the actual concentration is greater/lesser than C_0. Fig. 3 represents C with D^{-1}. Lesser the permeability of the porous medium smaller the actual concentration in the flow region. Fig.7 represents C with chemical reaction parameter γ. It is found that the actual concentration reduces in the degenerating chemical reaction case and enhances in the generating chemical reaction case. The micro rotation (ω) is shown in Figs for different parametric values. Fig. 4 represents ω with D^{-1}. It is found that lesser the permeability of the porous medium ($D^{-1} \leq 5 \times 10^2$) smaller the micro rotation ω and for further lowering of the permeability ($D^{-1} \geq 7 \times 10^2$) micro rotation depreciates in the entire flow region except in narrow adjacent to r=1. Fig. 5 represents the micro rotation (ω) with Hartmann number M. It can be seen from the profiles that higher the Lorentz force smaller the micro rotation ω. Fig. 8 represents ω with chemical reaction parameter γ. It is found that the micro rotation the magnitude of ω enhances in both the degenerating and generating cases.

The rate of heat transfer (Nusselt number) (Nu) at r=1 and r=2 is shown in Tables 1-4 for different parametric values. It can be seen from the profiles that an increase in G enhances |Nu| at r=1 and reduces at r=2. The variation of Nu with M and D^{-1} shows that higher the Lorentz force/lesser the permeability of the porous medium smaller the rate of heat transfer from both the cylinders. Also |Nu| enhances with increase in |N| at r=1 and reduces exponentially at both the cylinders. An increase in suction parameter S reduces |Nu| at the outer cylinder at r=1. The variation of Nu with micro rotation parameter λ and viscosity ratio parameter Δ shows that |Nu| enhances with λ and depreciates with Δ at r=1 and 2. The variation of Nu with Ec shows that higher the dissipative heat smaller |Nu| and for further dissipative heat Ec ≥ 0.5 larger |Nu| at both the cylinders. Also |Nu| experiences and enhances at r=1 and 2, with increase in the chemical reaction parameter γ.

The rate of mass transfer (Sherwood number) at r=1 and 2 is exhibited in Tables 5-8 for different parametric values. It is found that the rate of mass transfer enhances at both the cylinders with increase in |G|. Higher the Lorentz force/lesser the permeability of the porous medium larger |Sh| at r=1 and smaller at r=2. The variation of Sh with buoyancy ratio N shows that when the molecular buoyancy force dominates over the thermal buoyancy force |Sh| enhances when the buoyancy forces are in the same direction and for the forces acting in opposite direction it depreciates at both the cylinders. We find that the rate of mass transfer enhances with λ and Ec and reduces with Δ at r=1 and 2. The variation of Sh with Schmidt number Sc shows that lesser the molecular permeability larger |Sh| at r=1 and 2. Higher the porosity of the boundary (s) smaller the rate of mass transfer at r=1 and 2. With respect to γ we find that |Sh| enhances at both the cylinders in degenerating and generating chemical reaction cases.

The couple stress (Cw) at the inner and outer cylinders is exhibited in Tables 9-12 for different parametric values. It is found that Cw enhances with increase in |G| at r=1 and 2. Lesser the permeability of the porous medium larger the Cw of both the cylinders. The variation of Cw with magnetic parameter M shows that |Cw| depreciates with increase in M ≤ 5 and enhances with higher M ≥ 10.With respect to buoyancy ratio N we find that |Cw| enhances at r=1 and reduces at r= 2 with increase in N>0 and for an increase in |N| (<0) we notice a depreciation |Cw| at both the cylinders. Also higher the porosity of the boundary larger |Cw| at r=1 and 2. An increase in micro rotation parameter λ results in an enhancement in |Cw| at both the cylinders. With respect to viscosity ratio parameter Δ we find that |Cw| enhances at r=1 and 2 with increase in Δ ≤ 3 and for higher Δ ≥ 5 |Cw| enhances at r=1 and reduces at r=2. With reference to Eckert number Ec it can be seen that |Cw| enhances with increase in Ec ≤ 0.3 and reduces with higher Ec ≥ 0.5. The variation of Cw with chemical reaction parameter γ shows that |Cw| at r=1 enhances with γ ≤ 0.5 and depreciates with higher γ ≥ 1.5 at r=2 and reduces with γ for all G.

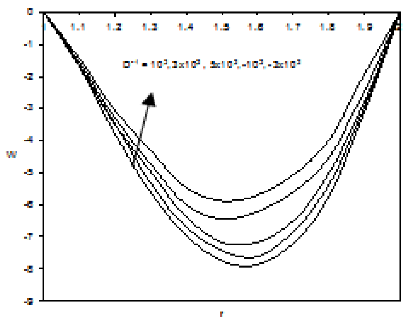

Fig. 1: Variation of w with D^{-1}
$G=10^3$, $M = 2$, $\gamma = 0.5$, $S=0.3$, $N=1$, $Ec=0.01$

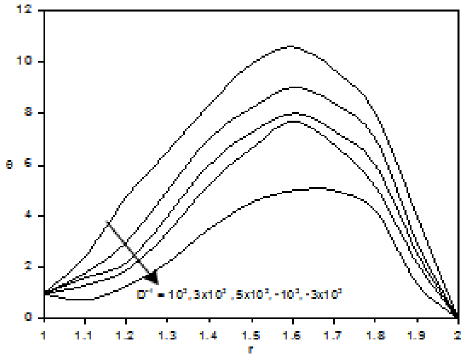

Fig. 2: Variation of θ with D^{-1}
$G=10^3$, $M = 2$, $\gamma = 0.5$, $S=0.3$, $N=1$, $Ec=0.01$

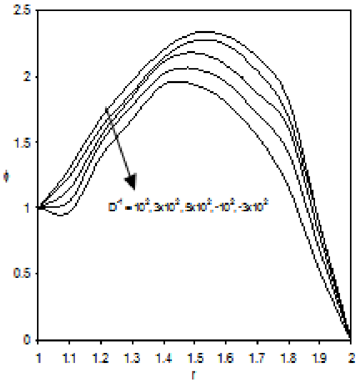

Fig. 3: Variation of C with D^{-1}
$G=10^3$, $M = 2$, $\gamma = 0.5$, $S=0.3$, $N=1$, $Ec=0.01$

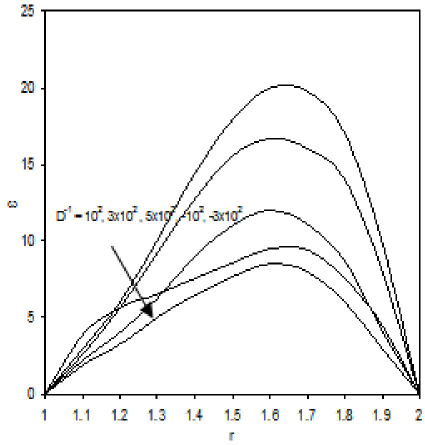

Fig. 4: Variation of ω with D^{-1}
$G=10^3$, $M = 2$, $\gamma = 0.5$, $S=0.3$, $N=1$, $Ec=0.01$

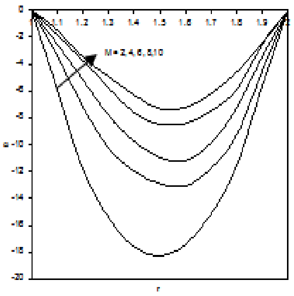

Fig. 5: Variation of ω with M

$G=10^3$, $D^{-1} = 10^2$, $M = 2$, $S=0.3$, $N=1$, $Ec=0.01$

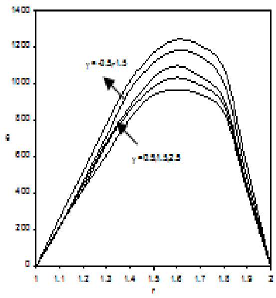

Fig. 6: Variation of θ with γ

$G=10^3$, $D^{-1} = 10^2$, $\gamma = 0.5$, $S=0.3$, $N=1$, $Ec=0.01$

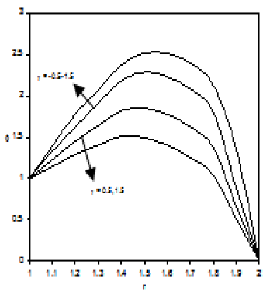

Fig. 7: Variation of C with γ

$G=10^3$, $D^{-1} = 10^2$, $M = 2$, $S=0.3$, $N=1$, $Ec=0.01$

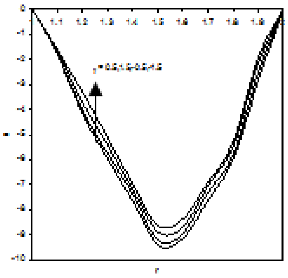

Fig. 8: Variation of ω with γ
$G=10^3$, $D^{-1}=10^2$, $M=2$, $S=0.3$, $N=1$, $Ec=0.01$

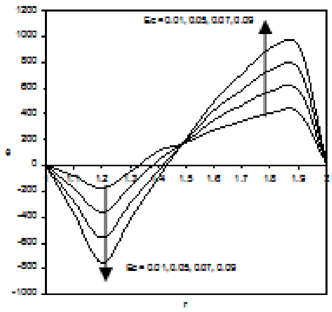

Fig. 9: Variation of θ with Ec
$G=10^3$, $D^{-1}=10^2$, $M=2$, $\gamma=0.5$, $S=0.3$, $N=1$

Table 1: Nusselt number (Nu) AT r = 1

G	I	II	III	IV	V	VI	VII	VIII	IX	X
10^2	2863.69	2854.17	2846.61	4165.76	1730.45	6417.56	-85.9243	17.8761	2484.45	2463.69
2×10^2	11365.3	11327.3	11297.2	16548.4	6846.43	25562.8	723.775	129.755	9845.58	9665.3
-10^2	2827.85	2818.44	2810.97	4104.71	1708.7	6363.72	263.515	17.8761	2453.4	2447.85
-2×10^2	11293.6	11255.9	11225.9	16426.3	6802.93	25455.1	706.098	122.879	9783.47	9693.6
D^{-1}	20	30	50	20	20	20	20	20	20	20
M	5	5	5	3	10	5	5	5	5	5
N	1	1	1	1	1	2	-0.5	-0.8	1	1
S	0.5	0.5	0.5	0.5	0.5	0.5	0.5	0.5	0.6	0.8

Table 2: Nusselt number (Nu) AT r = 1

G	I	II	III	IV	V	VI	VII	VIII	IX
10^2	2771.43	2863.69	2961.39	1778.82	1035.82	1835.57	2863.69	2875.62	2885.52
2×10^2	10997.3	11365.3	11754.9	7027.17	4062.09	7252.83	11365.3	11412.8	11452.2
-10^2	2736.66	2827.85	2924.41	1744.34	1008.24	1799.74	2827.85	2839.61	2849.28
-2×10^2	10927.8	11293.6	11681.0	6958.22	4006.92	7181.16	11293.6	11340.8	11379.7
Λ	0.01	0.03	0.05	0.03	0.03	0.03	0.03	0.03	0.03
Δ	1	1	1	3	5	1	1	1	1
Ec	0.1	0.1	0.1	0.1	0.1	0.3	0.5	0.1	0.1
Γ	0.2	0.2	0.2	0.2	0.2	0.2	0.2	0.5	1.5

Table 3: Nusselt number (Nu) AT r = 2

G	I	II	III	IV	V	VI	VII	VIII	IX	X
10^2	- 5123.67	-5092.03	- 5066.95	- 8963.87	- 2674.82	- 11548.9	-150.12	- 1.63865	- 4061.96	- 5123.67
2×10^2	- 20422.0	-20295.7	- 20195.6	- 35755.2	- 10649.6	- 46088.6	- 1242.77	-189.09	- 16186.4	- 20422.0
-10^2	- 5055.93	- 5024.566	-4999.7	- 8868.49	- 2630.03	- 11447.0	- 432.603	- 1.63865	- 4005.99	- 5055.93
-2×10^2	- 20286.6	-20160.8	- 20061.1	- 35564.4	- 10560.0	- 45884.8	- 1209.77	- 176.575	- 16074.4	- 20286.6
D^{-1}	20	30	50	20	20	20	20	20	20	20
M	5	5	5	3	10	5	5	5	5	5
N	1	1	1	1	1	2	-0.5	-0.8	1	1
S	0.5	0.5	0.5	0.5	0.5	0.5	0.5	0.5	0.6	0.8

Table 4: Nusselt number (Nu) AT r = 2

G	I	II	III	IV	V	VI	VII	VIII	IX
10^2	-4958.15	-5123.67	-5299.09	-4083.63	-2805.2	-3307.2	-5123.67	-5177.78	-5227.3
2 x 10^2	-19762.4	-20422.0	-21121.1	-16279.2	-11179.3	-13156.1	-20422.0	-20638.0	-20835.5
-10^2	-4892.89	-5055.93	-5228.72	-4033.28	-2769.11	-3239.47	-5055.93	-5109.55	-5158.56
-2 x 10^2	-19631.9	-20286.6	-20980.3	-16178.6	-11107.4	-13020.7	-20286.6	-20501.5	-20698.1
Λ	**0.01**	**0.03**	**0.05**	**0.03**	**0.03**	**0.03**	**0.03**	**0.03**	**0.03**
Δ	**1**	**1**	**1**	**3**	**5**	**1**	**1**	**1**	**1**
Ec	**0.1**	**0.1**	**0.1**	**0.1**	**0.1**	**0.3**	**0.5**	**0.1**	**0.1**
Γ	**0.2**	**0.2**	**0.2**	**0.2**	**0.2**	**0.2**	**0.2**	**0.5**	**1.5**

Table 5: Sherwood number (Sh) AT r = 1

G	I	II	III	IV	V	VI	VII	VIII
10^2	4.20652	4.19081	4.17831	7.86719	2.18338	6.77591	1.70382	-0.909843
2 x 10^2	9.32288	9.29145	9.26646	16.6442	5.27661	14.4617	1.6147	0.0730681
-10^2	-6.0262	-6.01044	-5.99799	-9.68688	-4.00307	-8.5956	-2.42457	-0.909843
-2 x 10^2	-11.1426	-11.1111	-11.0861	-18.4639	-7.0963	-16.2813	-3.43439	-1.89276
D^{-1}	**20**	**30**	**50**	**20**	**20**	**20**	**20**	**20**
M	**5**	**5**	**5**	**3**	**10**	**5**	**5**	**5**
N	**1**	**1**	**1**	**1**	**1**	**2**	**-0.5**	**-0.8**

Table 6: Sherwood number (Sh) AT r = 1

G	I	II	III	IV	V	VI	VII
10^2	4.07671	4.20652	4.34306	4.05888	3.08103	4.20583	4.20652
2 x 10^2	9.06309	9.32288	9.5962	9.02761	7.0719	9.32151	9.32288
-10^2	-5.89604	-6.0262	-6.16322	-5.87857	-4.90072	-6.02552	-6.0262
-2 x 10^2	-10.8824	-11.1426	-11.4164	-10.8473	-8.89159	-11.1412	-11.1426
Λ	**0.01**	**0.03**	**0.05**	**0.03**	**0.03**	**0.03**	**0.03**
Δ	**1**	**1**	**1**	**3**	**5**	**1**	**1**
Ec	**0.1**	**0.1**	**0.1**	**0.1**	**0.1**	**0.3**	**0.5**

Table 7: Sherwood number (Sh) AT r = 1

G	I	II	III	IV	V	VI	VII	IX
10^2	4.20652	11.8811	26.8038	41.9397	3.2232	1.5148	3.40474	2.96652
2 x 10^2	9.32288	24.672	54.5174	84.7892	7.40534	4.12826	7.88184	6.30228
-10^2	-6.0262	-13.7007	-28.6235	-43.7594	-5.14106	-3.71214	-5.54946	-2.9602
-2 x 10^2	-11.1426	-26.4916	-56.3371	-86.6089	-9.32319	-6.3256	-10.0260	-6.3026
Sc	**0.24**	**0.6**	**1.3**	**2.01**	**1.3**	**1.3**	**1.3**	**1.3**
Γ	**0.2**	**0.2**	**0.2**	**0.2**	**0.5**	**1.5**	**0.2**	**0.2**
S	**0.5**	**0.5**	**0.5**	**0.5**	**0.5**	**0.5**	**0.6**	**0.8**

Table.8: Sherwood number (Sh) AT r = 2

G	I	II	III	IV	V	VI	VII	VIII
10^2	-10.7802	-10.744	-10.7154	-14.591	-7.65431	-15.4088	-3.60985	-1.59979
2 x 10^2	-19.9605	-19.8883	-19.8309	-27.5822	-13.7088	-29.2177	-6.07476	-3.2976
-10^2	7.58058	7.54447	7.51578	11.3914	4.45473	12.2092	1.08519	-1.59979
-2 x 10^2	16.761	16.6887	16.6313	24.3826	10.5092	26.0181	2.87518	0.0980265
D^{-1}	**20**	**30**	**50**	**20**	**20**	**20**	**20**	**20**
M	**5**	**5**	**5**	**3**	**10**	**5**	**5**	**5**
N	**1**	**1**	**1**	**1**	**1**	**2**	**-0.5**	**-0.8**

Table 9: Sherwood number (Sh) AT r = 2

G	I	II	III	IV	V	VI	VII
10^2	-10.4996	-10.7802	-11.0741	-8.46992	-6.51564	-10.7794	-10.8802
2×10^2	-19.399	-19.9605	-20.5489	-15.34	-11.4315	-19.959	-19.9865
-10^2	7.29926	7.58058	7.87546	5.27034	3.31607	7.5798	7.62058
-2×10^2	16.1987	16.761	17.3503	12.1405	8023192	16.7594	16.8268
Λ	**0.01**	**0.03**	**0.05**	**0.03**	**0.03**	**0.03**	**0.03**
Δ	**1**	**1**	**1**	**3**	**5**	**1**	**1**
Ec	**0.1**	**0.1**	**0.1**	**0.1**	**0.1**	**0.3**	**0.5**

Table.10: Sherwood number (Sh) AT r = 2

G	I	II	III	IV	V	VI	VII	IX
10^2	-10.7802	-24.5507	-51.3268	-78.4854	-8.70407	-5.59123	-9.50985	-8.7802
2×10^2	-19.9605	-47.5016	-101.054	-155.371	-15.8496	-9.70594	-17.2259	-12.9605
-10^2	7.58058	21.3511	48.1272	75.1272	5.58693	2.63819	5.92232	8.68258
-2×10^2	16.761	44.3021	97.8542	152.171	12.7324	6.7529	13.6384	12.7668
Sc	**0.24**	**0.6**	**1.3**	**2.01**	**1.3**	**1.3**	**1.3**	**1.3**
Γ	**0.2**	**0.2**	**0.2**	**0.2**	**0.5**	**1.5**	**0.2**	**0.2**
S	**0.5**	**0.5**	**0.5**	**0.5**	**0.5**	**0.5**	**0.6**	**0.8**

Table11: Micro Rotation (Cw) AT r = 1

G	I	II	III	IV	V	VI	VII	VIII	IX	X
10^2	-2.36265	-2.41396	-2.45481	13.6062	-10.0714	-3.51208	10.7405	8.4906	-3.23332	-3.36265
2×10^2	-4.7253	-4.82793	-4.90962	27.2123	-20.1428	-7.02416	-1.2770	-0.587347	-6.46664	-1.6253
-10^2	2.36265	2.41396	2.45481	-13.6062	10.0714	3.51208	0.766203	-8.4906	3.23322	3.36065
-2×10^2	4.7253	4.82793	4.90962	-27.2123	20.1428	7.02416	1.27701	0.587347	6.46664	7.6253
D^{-1}	**20**	**30**	**50**	**20**	**20**	**20**	**20**	**20**	**20**	**20**
M	**5**	**5**	**5**	**3**	**10**	**5**	**5**	**5**	**5**	**5**
N	**1**	**1**	**1**	**1**	**1**	**2**	**-0.5**	**-0.8**	**1**	**1**
S	**0.5**	**0.5**	**0.5**	**0.5**	**0.5**	**0.5**	**0.5**	**0.5**	**0.6**	**0.8**

Table 12: Micro Rotation (Cw) AT r = 1

G	I	II	III	IV	V	VI	VII	VIII	IX
10^2	-2.28418	-2.36265	-2.43565	15.4633	19.6606	-2.36553	-2.36265	-2.28804	-2.15174
2×10^2	-4.56835	-4.7253	-4.87131	30.9266	39.3213	-4.73106	-4.7253	-4.57607	-4.30348
-10^2	2.28418	2.36265	2.43565	-15.4633	-19.6606	2.36553	2.3265	2.28804	2.15174
-2×10^2	4.56835	4.7253	4.87131	-30.9266	-39.3213	4.73106	4.7253	4.57607	4.30348
Λ	**0.01**	**0.03**	**0.05**	**0.03**	**0.03**	**0.03**	**0.03**	**0.03**	**0.03**
Δ	**1**	**1**	**1**	**3**	**5**	**1**	**1**	**1**	**1**
Ec	**0.1**	**0.1**	**0.1**	**0.1**	**0.1**	**0.3**	**0.5**	**0.1**	**0.1**
Γ	**0.2**	**0.2**	**0.2**	**0.2**	**0.2**	**0.2**	**0.2**	**0.5**	**1.5**

Table 13: Micro Rotation (Cw) AT r = 2

G	I	II	III	IV	V	VI	VII	VIII	IX	X
10^2	0.524561	0.579606	0.623347	-7.67982	5.8893	0.726085	-2.7248	-2.46984	0.991506	1.04561
2×10^2	1.04912	1.15921	1.24669	-15.3596	11.7786	1.45217	0.444549	0.323634	1.98301	2.04912
-	-	-	-	7.6798	-	-	-2.7248	2.46984	-	-

10^2	0.524561	0.579606	0.623347	2	5.8893	0.726085			0.991506	1.02459
-2 x 10^2	-1.04912	-1.15921	-1.24669	15.3596	-11.7786	-1.45217	-0.444549	-0.323634	-1.98301	-2.04912
D^{-1}	**20**	**30**	**50**	**20**	**20**	**20**	**20**	**20**	**20**	**20**
M	**5**	**5**	**5**	**3**	**10**	**5**	**5**	**5**	**5**	**5**
N	**1**	**1**	**1**	**1**	**1**	**2**	**-0.5**	**-0.8**	**1**	**1**
S	**0.5**	**0.5**	**0.5**	**0.5**	**0.5**	**0.5**	**0.5**	**0.5**	**0.6**	**0.8**

Table 14: Micro Rotation (Cw) AT r = 2

G	I	II	III	IV	V	VI	VII	VIII	IX
10^2	0.511065	0.524561	0.534492	-2.62255	-0.944216	0.526132	0.524561	0.407475	0.232278
2 x 10^2	1.02213	1.04912	1.06898	-5.2451	-1.88843	1.05226	1.04912	0.81495	0.464555
-10^2	-0.511065	-0.524561	-0.534492	2.62255	0.944216	-0.526132	-0.524561	-0.4.7475	-0.232278
-2 x 10^2	-1.02213	-1.04912	-1.06898	-5.2451	1.88843	-1.05226	-1.04912	-0.81495	-0.464555
λ	**0.01**	**0.03**	**0.05**	**0.03**	**0.03**	**0.03**	**0.03**	**0.03**	**0.03**
Δ	**1**	**1**	**1**	**3**	**5**	**1**	**1**	**1**	**1**
Ec	**0.1**	**0.1**	**0.1**	**0.1**	**0.1**	**0.3**	**0.5**	**0.1**	**0.1**
γ	**0.2**	**0.2**	**0.2**	**0.2**	**0.2**	**0.2**	**0.2**	**0.5**	**1.5**

VI. CONCLUSIONS:

- An increasing in |G| enhances the axial velocity |w|, temperatureθ, concentration C and angular velocity ω an entire flow region.
- Lesser the permeability of porous medium Lorentz force reduces w, θ, C and ω in the flow region.
- The velocity, the temperature and micro rotation enhances in both generating and degenerating chemical reaction cases.
- While the concentration reduces in the degenerating chemical reaction case and enhances in the generating case.
- An increasing Eckert number Ec enhances in the velocity and reduces the actual temperature. The concentration reduces with increasing Sc.
- An increasing |G| enhances the rate of heat transfer, mass transfer and couple stress at both the cylinders. An increasing M and D^{-1} enhances |Nu| at both cylinders. They enhances |Sh| at r=1, and reduce at r=2. Where |Cw| enhances with D^{-1} at r=1, and 2.
- An increasing N>0 enhances |Nu| at r=1, |Sh| at r=1 and 2, |Cw| at r=1 and reduces |Nu| at r=2, |Cw| at r=2. While an increasing |N| enhance |Nu| at r=1 and reduces at r=2, |sh|, |Cw| at r=1 and 2.
- |Nu|, |Sh| and |Cw| at r=1 and r=2 both degenerating and generating chemical reaction cases.
- An increasing the micropolar parameter λ enhances |Nu|, |Sh| and |Cw| at both the cylinders.
- An increasing viscosity ratio parameter Δ reduces |Nu|, |Sh| and enhances |Cw| at both the cylinders.
- Higher the dissipative heat larger |Sh|, |Cw| and smaller |Nu| at r=1 and 2. An increasing suction parameter S reduces |Cw| and enhances |Nu|, |Sh| at both the cylinders.

REFERENCES:

[1]. Agarwal R.S. and Dhanpal C.: Numerical solution of micropolar fluid flow and heat transfer between two co-axial porous circular cylinders. Int. J. Eng. Sci., 26(11) pp. 1133-1142 (1988).

[2]. Barletta A., Magyari E., Lazzari S. and Pop I.: Closed from solutions for mixed convection with magneto hydro dynamic effect in a vertical porous annulus surrounding an electric cable. J. Heat Transfer, 131, 6, (2009).

[3]. Barletta A.: Int. J. Heat Mass Transfer, Vol. 40, pp. 15-26 (1997).

[4]. Barletta A.: Int. J. Heat Mass Transfer, Vol. 42, pp. 2243-2253, (1999).

[5]. Eringen A.C.: The theory of micropolar fluids – theory and application. Birkhauser, Bostan (1966).

[6]. El-Hakein M.A.: Int. Comns. Heat Mass Transfer, Vol. 27, pp. 581-590 (2000).

[7]. Fand R.M. and Brucker J.: Int. J. Heat and Mass Transfer. p. 723 (1986).
[8]. Grosan T., Revnic C., Pop I. and Ham D.B.: Magnetic field and internal heat generation effects on the free convection in a rectangular cavity filled with a porous medium. Int. J. Heat Mass Transfer, 52 (5-6). pp. 1525-1533(2009).
[9]. GiampietroI Fabbri: Int. J. Heat and Mass Transfer, p. 3003 (2004).
[10]. Gebhart B.J.: Fluid Mech., Vol. 14, pp. 225-232, (1962).
[11]. Gebhart B. and Mollendorf J.: Fluid Mech., Vol. 38, pp. 107 (1969).
[12]. Lukaszewicz G.: Micropolar fluids, theory and applications, Birkhauser, Bostan (1999).
[13]. Murthy D.V.S. and Singh P.: Int. J. Heat and Mass Transfer, (1997).
[14]. Murthy J.V.R. and Bahali N.K.: Steady flow of micropolar fluid through a circular pipe under a transverse magnetic field with constant suction/injection, (2009).
[15]. Nakayama A. and Pop I.: Int. Communications in Heat and Mass Transfer, (1989).
[16]. Okada K. and Ozoe H.: Experimental heat transfer rates of natural convection of molten Gallium suppressed under an external magnetic field in Either the x, y or z Direction. J. Heat Transfer, 14 (1) pp. 107-114(1992).
[17]. Oreper G.M. and Szekely J.: The effect of an externally imposed magnetic field on buoyancy driven flow in a rectangular cavity. J. Crystal Growth, 64 (3), pp. 505-515, (1983).
[18]. Prasad V., Kulacki F.A. and Kulakarni A.V.: Free convection in a vertical, porous annulus with constant heat flux on the inner wall-experimental results. Int. J. Heat Mass Transfer, 29, pp. 713-723 (1986).
[19]. Panja S., Sengupta P.R. and Debnath L.: Hydro magnetic flow of Reiner – Rivlin fluid between two coaxial circular in cylinders with porous walls. Computers Math. Applic. 32 (2). pp. 1-4, (1986).
[20]. Prasad V. and Kulacki F.A.: Free convection heat transfer in a liquid-filled vertical annulus. ASME J. Heat Transfer, 107, pp. 596 (1985).
[21]. Sankar M., Venkatachalappa M. and Shivakumara I.S.: Effect of magnetic field on natural convection in a vertical cylindrical annulus. Int. J. Eng. Science, 44, pp. 1556-1570 (2006).
[22]. Shivakumara I.S., Prasanna B.M.R., Rudraiah N. and Venkatachalappa M.: Numerical study of natural convection in a vertical cylindrical Annulus using a Non-Darcy equation, J. porous Media, 5(2). pp. 87-1-2 (2002).
[23]. Shivashankar H.S., Prasanna B.M.R., Sankar M. and Sreedhara S.: Numerical study of natural convection in vertical porous Annuli in the presence of magnetic field, (2009).
[24]. Soundalgekar V.M. and Jaisawal B.S.D., Uplekar A.G. and Takhar H.S.: Appl. Mech and Engg, Vol. 4, pp. 203-218 (1999).
[25]. Sreevani M.: Mixed convective heat and mass transfer through a porous medium in channels with dissipative effects Ph.D. Thesis, S.K. University, Anantapur (A.P.), (2003).
[26]. Soundalgekar V.M. and Pop I.: Int. J. Heat Mass Transfer, Vol. 17, pp. 85-90 (1974).
[27]. Verma P.D.S. and Singh M.: Magnetic fluid flow through porous annulus. Int. J. Non-linear Mech., 16(314), pp. 371-37 (1981).

IOSR Journal of Engineering (IOSRJEN) is UGC approved Journal with Sl. No. 3240, Journal no. 48995.

Dr.K.Gnanaprasunamba "MHD Double Diffusive Convective Heat Transfer Flow Of Micropolar Fluid In Cylindrical Annulus .IOSR Journal of Engineering (IOSRJEN), vol. 08, no. 6, 2018, pp. 01-14.